Signal processing and recognition of true kinetic equations containing non-integer derivatives from raw dielectric data

Article *in* Signal Processing · November 2003

DOI: 10.1016/S0165-1684(03)00195-6 · Source: DBLP

CITATIONS
23

READS
74

2 authors:

Raoul Rashid Nigmatullin
Kazan National Research Technical University
295 PUBLICATIONS **4,711** CITATIONS

SEE PROFILE

Sergey Osokin
Kazan (Volga Region) Federal University
14 PUBLICATIONS **159** CITATIONS

SEE PROFILE

Available at
www.ComputerScienceWeb.com
POWERED BY SCIENCE DIRECT

Signal Processing 83 (2003) 2433–2453

SIGNAL PROCESSING

www.elsevier.com/locate/sigpro

Signal processing and recognition of true kinetic equations containing non-integer derivatives from raw dielectric data

R.R. Nigmatullin*, S.I. Osokin

Department of Theoretical Physics, Kazan State University, 420008 Kazan, Tatarstan, Russia

Received 3 December 2002

Abstract

Signal processing in dielectric spectroscopy implies that it is necessary to find a 'true' fitting function (having a certain physical meaning), which describes well the complex permittivity and impedance data. In dielectric spectroscopy for description of complex permittivity/impedance data researches usually use the empirical Cole–Davidson (CD) and Havriliak–Negami (HN) equations that contains one relaxation time. But the parameters figuring in CD and HN equations do not have clear physical meaning as well as fitting parameters entering into linear combination of several CD or HN equations. For description of dielectric (especially asymmetric) spectra we suggest the complex permittivity functions containing two or more characteristic relaxation times. These complex susceptibility functions correspond in time domain to new type of kinetic equation containing non-integer (fractional) integrals and derivatives. We suppose that these kinetic equations describe a wide class of dielectric relaxation phenomena taking place in heterogeneous substances. To support and justify this statement the special recognition procedure has been developed that helps to identify this new kinetic equation from raw dielectric data. It incorporates the *ratio presentation* (or RP) format and separation procedure. Separation procedure was turned out to be helpful in detection of number of relaxation processes (each process is described by a characteristic relaxation time) taking place in the dielectric material under consideration. We suppose that this procedure can be applicable also for identification of fractal noises.

PACS: 61.25.Em; 77.22.Gm; 05.40. − a; 02.60.Ed.; 06.20.Dk.; 07.05.Kf

Keywords: Dielectric spectroscopy; Ratio presentation; Kinetic equations; Fractional integrals; Fractional derivatives

1. Introduction

Signal processing in dielectric spectroscopy implies description of a complex permittivity function and impedance in terms of an analytical function. Most of the experimental studies show that the dielectric ac response in many dielectric materials especially for glass-forming materials is hardly being explained by the "classical" Debye dielectric function [3,7–11,21,23–25]

$$\varepsilon(\mathrm{j}\omega) = \varepsilon'(\omega) - \mathrm{j}\varepsilon''(\omega) = \varepsilon_\infty + \frac{\varepsilon(0) - \varepsilon_\infty}{1 + \mathrm{j}\omega/\omega_\mathrm{p}}. \qquad (1)$$

Generally, the experimentally observed non-Debye ac response of glass-forming hydrogen-bonded substances as well as that of a variety of solid dielectric materials in a remarkable wide range of frequencies have been found to exhibit much more broadening in

* Corresponding author.
E-mail address: nigmat@knet.ru (R.R. Nigmatullin).

0165-1684/$ - see front matter © 2003 Elsevier B.V. All rights reserved.
doi:10.1016/S0165-1684(03)00195-6

its loss curves and in many cases suffers from *asymmetry*. The most conventional empirical analytical dielectric expression that is often used to describe the generalized broadened asymmetric relaxation loss peak observed in many dielectric materials over a wide frequency range is the conventional Havriliak–Negami (HN) equation [25,8,6]

$$\chi_{\mathrm{HN}}(\mathrm{j}\omega) = \chi'(\omega) - \mathrm{j}\chi''(\omega) = (\varepsilon(\mathrm{j}\omega) - \varepsilon_\infty)/\varepsilon_0 = \frac{\varepsilon(0) - \varepsilon_\infty}{[1 + (\mathrm{j}\omega/\omega_\mathrm{p})^v]^\beta}, \tag{2}$$

where $\chi_{\mathrm{HN}}(\mathrm{j}\omega)$ is the HN complex susceptibility with the real and imaginary components $\chi'(\mathrm{j}\omega)$ and $\chi''(\mathrm{j}\omega)$, respectively, and $\varepsilon_0 = 8.854 \times 10^{-12}$ F/m is the permittivity of free space. The parameter v $(0 < v \leqslant 1)$ is a measure of the broadness of a symmetric dielectric relaxation curve and β $(0 < \beta \leqslant 1)$ is the shape parameter of an asymmetric relaxation curve. The relaxation curve with $\beta = v = 1$ corresponds to the "ideal" Debye-type ac response. When $\beta = 1$, the HN-equation reduces to the well-known Cole–Cole (CC) empirical dielectric function. Another non-Debye dielectric behavior is obtained from the HN-expression for $v = 1$, which is known as the Cole–Davidson (CD) empirical function. Here, this type of behavior will be collectively termed as the *Debye-type* response [19]. It has been reported [11] that the experimental ac relaxation curves of water–polymer mixtures can be described by the CC-dielectric function. On the other hand, the regime close to the so-called α-relaxation peaks in the observed loss–frequency curves of glass-forming glycerol and propylene carbonate (PC) has been described [10,23] well by the CD empirical equation. However, in water mixtures with small organic compounds such as polyhydroxyl alcohol [21] the primary dielectric relaxation process exhibiting a broad and asymmetric relaxation curve has been described by the Fourier transform of the Kohlrausch–Williams–Watts (KWW) function [21,25,8] that gives the complex permittivity function in the form

$$\varepsilon(\mathrm{j}\omega) = \varepsilon_\infty + [\varepsilon(0) - \varepsilon_\infty] \int_0^\infty [-\mathrm{d}\Phi(t)/\mathrm{d}t] \times \exp(-\mathrm{j}\omega t)\,\mathrm{d}t \tag{3a}$$

with

$$\Phi(t) = \exp\lfloor -(t/\tau)^{\beta_K} \rfloor, \tag{3b}$$

where the parameter β_K $(0 < \beta_K \leqslant 1)$ is a measure of the broadness of an asymmetric loss relaxation curve. It is worth noting here that the Fourier transform of Eq. (3a) into the frequency domain cannot be expressed in the form of a simple algebraic expression and so can be evaluated only numerically [8] and this KWW function is not usually highly applicable for describing dielectric behavior in some materials.

Other empirical expressions can be also used to analyze the experimental ac response of dielectrics over a wide range of frequencies, is the widely used the Jonscher's formula [8] that describes the frequency dependence of $\chi''(\omega)$ of the complex susceptibility below and above the loss-peak angular frequency ω_p.

Another empirical permittivity function, which includes all of Jonscher's "universal response," the Debye-, CC-, and CD-dielectric functions as its special cases and which also takes into account the contribution of dc conduction, which may be encountered experimentally at the low-frequency side, has been recently proposed by Raicu [19]

$$\varepsilon(\mathrm{j}\omega) = \varepsilon_\infty + \frac{\sigma}{\mathrm{j}\omega} + \frac{\varepsilon(0) - \varepsilon_\infty}{[(\mathrm{j}\omega\tau)^\alpha + (\mathrm{j}\omega\tau)^{1-\beta}]^\gamma}. \tag{4}$$

Traditionally, the measured ac permittivity-frequency data is interpreted and analyzed quantitatively by the use of expression (2) or its linear combinations. To achieve such quantitative permittivity data analysis, some sort of a non-linear curve-fitting programs [5,18] to the model chosen are usually employed. Usually, the use of the empirical dielectric expressions is often criticized for they often involve adjustable parameters that are sometimes difficult to justify and understand their physical significance. Moreover, a conventional non-linear curve-fitting method usually results in a best curve fit to the experimental data with a number quantifying how good the fit is and yields a set of values for the adjustable parameters involved, which are always presumed to represent the behavior of such data. However, such fitting programs can fit, given enough adjustable variables, almost any theoretical/empirical model, but they cannot tell one which theory/model should apply. Consequently, the deduced fitting parameters might be *illusive* or *misleading*, as one often obtains different sets of values for them, corresponding to different "local" minima in the statistical function used in the minimization procedure, which give best

fits to the same model chosen. Only when a "global" minimum is arrived at through the minimization procedure, the obtained set of fitting parameters can be considered to be physically well behaved and reliable for further analysis. In general, it is rather difficult to develop some additional justified criteria which is helpful in differentiation of conventional or, in other words, the *imposed data curve-fitting* approach from an approach which does not contain initially supposed empirical functions and contains some verification criteria for justification of a "true" chosen hypothesis.

2. Formulation of the problem

For describing the asymmetric peaks in dielectric spectra we suggest to use new complex dielectric functions, which can be expressed as

$$\varepsilon(\mathrm{j}\omega) = \varepsilon_\infty + \frac{\varepsilon(0) - \varepsilon_\infty}{1 + R(\mathrm{j}\omega)}. \tag{5}$$

The complex function $R(\mathrm{j}\omega)$ is determined by the following expressions:

(a) for equivalent scheme with two recap elements (resistance+capacitance; they form one combined element with intermediate impedance properties between pure resistance and capacitance [13]) connected in parallel

$$R(\mathrm{j}\omega) = (\mathrm{j}\omega\tau_1)^{\nu_1} + (\mathrm{j}\omega\tau_2)^{\nu_2}, \tag{6a}$$

(b) for equivalent scheme with two recap elements connected in series

$$R(\mathrm{j}\omega) = [(\mathrm{j}\omega\tau_1)^{-\nu_1} + (\mathrm{j}\omega\tau_2)^{-\nu_2}]^{-1}. \tag{6b}$$

Here we want to stress one *principal feature* of these functions, viz., expressions (6) contain *two* characteristic relaxation times forming in the most cases one loss peak belonging to one function (5). These two relaxation times constitute one function and are formed *without* additive combinations of the two "simple" functions usually combined by the HN (2), KWW (3) or Raicu (4) functions containing only one parameter of relaxation. It is necessary to mark here that these complex functions (6) are *not* a new empirical supposition. They have been recognized with the use of special procedure initially suggested in papers [1].

Functions (6) incorporate a single *recap* element or combination of several *recaps* elements in order to reflect the *fractal* nature of a sample interior and/or interfacial/electrode phenomena [4] through a general impedance form having intermediate characteristics with a "fractional" power-law frequency response of the type [22,12,16,13]

$$Z_\nu(\mathrm{j}\omega) \equiv R_0(\mathrm{j}\omega\tau)^{-\nu}. \tag{7}$$

Here τ is considered as a characteristic relaxation time of a fractal subsystem, R_0 is a dimensional parameter. The power-law exponent is supposed to be located in the interval $0 \leqslant \nu \leqslant 1$, but in some cases it can be beyond of this interval [13]. Each *recap* element, besides its own exponent ν, is dominant in a certain frequency range $\omega_{\min} \leqslant \omega \leqslant \omega_{\max}$, which cannot be sometimes achieved by the experimental setup used; this frequency limit should reflect the existence of a fractal structure formed in many mesoscopic systems.

Let us consider the kinetic equation in fractional derivatives of the following type:

$$[\tau_1^{\nu_1} D_{t_0}^{\nu_1} + \tau_2^{\nu_2} D_{t_0}^{\nu_2}](P(t) - P(t_0)) + P(t) = 0. \tag{8}$$

Here $P(t)$ is a value of the total polarization, the operator D_a^q $(0 \leqslant q \leqslant 1)$ defines the Riemann–Liouville non-integer differential operator [17]

$$\begin{aligned} D_a^q f(x) &= \frac{\mathrm{d}}{\mathrm{d}x}\,[D_a^{q-1} f(x)] \\ &= \frac{\mathrm{d}}{\mathrm{d}x}\left[\frac{1}{\Gamma(1-q)}\int_a^x (x-y)^{-q} f(y)\,\mathrm{d}y\right]. \end{aligned} \tag{9}$$

The parameters $\tau_{1,2}$ determine some characteristic times, which provide the conservation of dimension in the both parts of Eq. (8). It is easy to find the stationary solution of the kinetic equation (8). We present the solution in the form

$$P(t) = \chi(\mathrm{j}\omega)\exp[\mathrm{j}\omega t]. \tag{10}$$

Taking into account the value of the integral

$$D^{v}_{-\infty}[\exp(j\omega t)] = \frac{d}{dt}\left[\frac{1}{\Gamma(1-v)}\int_{-\infty}^{t}(t-u)^{-v}e^{j\omega u}\,du\right] = (j\omega)^{v}\exp(j\omega t) \quad (11)$$

and initial condition $P(-\infty)=0$ it is easy to find the expression for complex susceptibility

$$\chi(j\omega) = \frac{\chi(0)}{1+(j\omega\tau_1)^{v_1}+(j\omega\tau_2)^{v_2}}. \quad (12)$$

This expression totally corresponds to the complex permittivity written in form (5) with complex function $R(j\omega)$ taken from (6a).

Let us consider another kinetic equation

$$[\tau_1^{-v_1}D_{t_0}^{-v_1}+\tau_2^{-v_2}D_{t_0}^{-v_2}](P(t)-P(t_0))+P(t) = 0. \quad (13a)$$

It can be presented also in equivalent form as

$$[\tau_1^{-v_1}D_{t_0}^{-v_1}+\tau_2^{-v_2}D_{t_0}^{-v_2}]^{-1}P(t)+(P(t)-P(t_0)) = 0. \quad (13b)$$

Here fractional exponents are supposed to be located in the interval ($0 \leqslant v_1,\ v_2 \leqslant 1$). Formally the last equation coincides with Eq. (8) but with one *essential* difference. It represents the kinetic equation containing the fractional *integral* operators. The linear combination of fractional integral operators taken in the inverse form leads again to a complex operator of fractional derivative. The stationary solution of this equation can be found by analogy with (8). At initial condition $P(-\infty)=\chi(0)\exp[j(\omega-j\varepsilon)t]$ ($\varepsilon\to 0$) [that corresponds to the adiabatic switching of the electric field at $t=-\infty$] it is easy to find the expression for complex susceptibility. It can be written as

$$\chi(j\omega) = \frac{[(j\omega\tau_1)^{-v_1}+(j\omega\tau_2)^{-v_2}]\chi(0)}{1+[(j\omega\tau_1)^{-v_1}+(j\omega\tau_2)^{-v_2}]} = \frac{\chi(0)}{1+[(j\omega\tau_1)^{-v_1}+(j\omega\tau_2)^{-v_2}]^{-1}} \quad (14)$$

and corresponds to the expression of the complex permittivity (5) with $R(j\omega)$ taken from (6b).

Generalizing kinetic equations (8) and (13) containing fractional derivatives one can expect the following general structure of kinetic equations describing the dielectric relaxation phenomenon in time domain for wide class of dielectric materials

$$\sum_{k=1}^{n}\tau_k^{v_k}D_{t_0}^{v_k}[P(t)-P(t_0)]+P(t)=0. \quad (15)$$

In partial cases ($n=1,\ v=1$ and $n=1,\ v\neq 1$) the last equation describes the known kinetics of Debye and Cole–Cole type. The physical meaning of the last kinetic equation is the following. We suppose that all relaxation system including a set of strongly correlated microdipoles can be divided on n subsystems. It might be a set of dipole clusters or ensemble of strongly correlated molecules. Each subsystem is interacting with thermostat with the help of collision/rotation mechanism, which is expressed by means of fractional derivative (the physical meaning of the fractional integral is discussed in [13]). Each subsystem k ($k=1,2,\ldots,n$) is characterized by a relaxation time τ_k showing the contribution of the chosen relaxation unit into the general process of relaxation. The number of subsystems, giving an additive contribution to the general picture of relaxation is defined by a structure of the concrete heterogeneous material considered. At an initial stage the kinetic equation (15) can be considered as a reasonable and phenomenological hypothesis, which is recognized from correct treatment of raw dielectric data. After identification of this type of kinetic equation on a wide class of heterogeneous materials the further theoretical attempts should be undertaken in explanation of their microscopic origin. We suppose that this equation describing the relaxation of the total polarization in a bulk material can serve a basis of signal processing in dielectric spectroscopy (DS).

The *main* purpose of this paper is to find and justify the procedures that can help to *recognize* this new type of kinetic equation in the process of treatment of raw DS data. If it becomes possible to identify this equation from analysis of DS data then decisive arguments can be found in prove that fractal kinetic equations *do* exist in Mother-Nature. It will help to reconsider and generalize the basic kinetic equations of statistical mechanics, which incorporates only integer derivatives and identify new relaxation phenomena that need for their description the operator of non-integer derivative

or their linear combination. The rest material of this paper is organized as follows. Section 3 describes the so-called ratio presentation (RP) format, which contains additional information for identification of relaxation processes taking place in low-frequency domain. The separation procedure outlined in Section 4 helps to identify a number of relaxation processes figuring in kinetic equation (15). In Section 5, we are analyzing real available DS data for complex susceptibility received from different laboratories. The last Section 6 is finishing this consideration by results and their discussion.

3. Ratio presentation format

In practice, it is necessary to differentiate between the so-called (low-frequency dispersion) LFD process ($\sim (1/(\mathrm{j}\omega\tau)^{\alpha})$, see also Table 1) and a relaxation process described by the Cole–Cole function, and to find a criterion that helps to detect a mixture of these (and other) possible processes from their separate contributions. A solution corresponding to these requirements can be realized with the use of the ratio

$$-\left(\frac{\mathrm{Re}[\varepsilon(\mathrm{j}\omega)]}{\mathrm{Im}[\varepsilon(\mathrm{j}\omega)]}\right) \equiv \frac{\mathrm{Re}[1/\varepsilon(\mathrm{j}\omega)]}{\mathrm{Im}[1/\varepsilon(\mathrm{j}\omega)]} = \cot(\varphi) + \frac{\varepsilon_{\infty}|D(\mathrm{j}\omega)|}{\Delta\varepsilon \sin(\varphi)}. \tag{16}$$

Here $\varepsilon(\mathrm{j}\omega) \equiv \mathrm{Re}[\varepsilon(\mathrm{j}\omega)] - \mathrm{j}\,\mathrm{Im}[\varepsilon(\mathrm{j}\omega)]$ and $D(\mathrm{j}\omega) \equiv |D(\mathrm{j}\omega)| \exp(\mathrm{j}\varphi) = 1 + R(\mathrm{j}\omega)$. The function $R(\mathrm{j}\omega)$ is defined by expression (5). We have explored the possibilities of this new format in the identification of individual processes and combinations of different processes.

Table 1
The relationship between the parameters of the low-frequency dispersion (LFD) and the Cole–Cole functions, and the parameters A, B, C from expressions (17) and (18)

LFD	$A = \cot\left(\frac{\pi\alpha}{2}\right)$
$\varepsilon(\mathrm{j}\omega) \equiv \varepsilon_{\infty} + \frac{1}{(\mathrm{j}\omega\tau)^{\alpha}}$	$B = \frac{\varepsilon_{\infty}(2\pi\tau)^{\alpha}}{\sin(\pi\alpha/2)}$
Cole–Cole	$A = \left(\frac{\varepsilon_s+\varepsilon_{\infty}}{\varepsilon_s-\varepsilon_{\infty}}\right)\frac{1}{\tan(\pi\nu/2)}$
$\varepsilon(\mathrm{j}\omega) = \varepsilon_{\infty} + \frac{\varepsilon_s-\varepsilon_{\infty}}{1+(\mathrm{j}\omega\tau)^{\nu}}$	$B = \frac{\varepsilon_s}{(\varepsilon_s-\varepsilon_{\infty})(2\pi\tau)^{\nu}\sin(\pi\nu/2)}$
	$C = \frac{\varepsilon_{\infty}(2\pi\tau)^{\nu}}{(\varepsilon_s-\varepsilon_{\infty})\sin(\pi\nu/2)}$

The LFD function in ratio format. If the function $D(\mathrm{j}\omega)$ defined by expression (16) coincides with the LFD function, then simple calculations lead to the expression

$$-\left(\frac{\mathrm{Re}[\varepsilon(\mathrm{j}\omega)]}{\mathrm{Im}[\varepsilon(\mathrm{j}\omega)]}\right) = A + Bf^{\alpha}. \tag{17}$$

The relationship between the parameters $A(\varepsilon_{\infty}, \tau, \alpha)$ and $B(\varepsilon_{\infty}, \tau, \alpha)$, and the conventional parameters ε_{∞}, $\sigma = 1/\tau^{\alpha}$ and α are given in Table 1. Fig. 1 shows the frequency dependence of function (17) for some concrete values of the fitting parameters ε_{∞}, σ and α. As one can see from the double-log scale representation, the LFD function appears as a straight sloping line when $\alpha = 1$ or as a broken straight line (with a region that is parallel part to the frequency axis) when $\alpha < 1$. The use of expression (17) for recognition of the existence of an LFD process becomes very simple. Moreover, the application of expression (17) effectively involves the *simultaneous* fitting of both the real and imaginary parts and therefore renders the whole fitting procedure much more reliable.

The Cole–Cole function in ratio format: If the function $D(\mathrm{j}\omega)$ coincides with the part of complex permittivity defining the pure Cole–Cole function ($D(\mathrm{j}\omega) \equiv 1 + (\mathrm{j}\omega\tau)^{\nu}$)

$$\varepsilon(\mathrm{j}\omega) = \varepsilon_{\infty} + \frac{\varepsilon(0) - \varepsilon_{\infty}}{1 + (\mathrm{j}\omega\tau)^{\nu}},$$

then the ratio has the form

$$-\left(\frac{\mathrm{Re}[\varepsilon(\mathrm{j}\omega)]}{\mathrm{Im}[\varepsilon(\mathrm{j}\omega)]}\right) = A + Bf^{-\nu} + Cf^{\nu}. \tag{18}$$

The relationships between the fitting parameters A, B, C and initial parameters defining the Cole–Cole function (i.e. ε_{∞}, $\Delta\varepsilon$, $\tau = 1/\omega_p$, ν) are given in Table 1. The principle difference between expressions (17) and (18) is the appearance of a low-frequency branch ($\sim B$) that helps to differentiate easily between the LFD process and the Cole–Cole relaxation process. Fig. 2 shows presentation (18) of the Cole–Cole function, for certain values of the fitting parameters in double-log scale. The appearance of the low-frequency branch transforms the shape of the ratio-format spectrum from

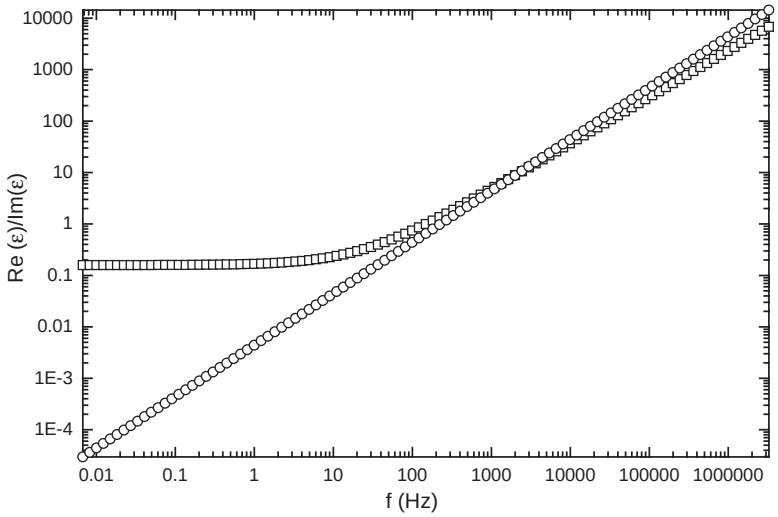

Fig. 1. Imitation of low-frequency dispersion (LFD) process. Circles represent the LFD function with $\alpha = 1$, $\tau_{\mathrm{LFD}} = 0.0001$, $\varepsilon_\infty = 7$, squares represent the LFD with $\alpha = 0.9$, $\tau_{\mathrm{LFD}} = 0.0001$, $\varepsilon_\infty = 7$.

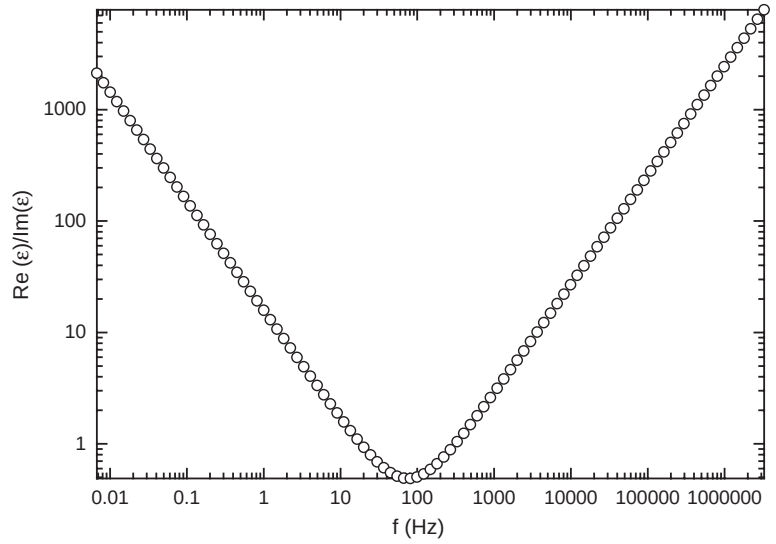

Fig. 2. The Cole–Cole function in the RP format with parameters $v = 0.98$, $\tau = 0.01$, $\varepsilon_s = 150$, $\varepsilon_\infty = 7$.

that of a broken line (characteristic of an LFD process) into a profile resembling the letter "V". We wish to stress here, that the function appears in the V-shaped form, even in cases, when the normal presentation exhibits only the tail of this process. It can be explained by the fact that the frequency minimum of this function is found from the relationship

$$f_{\mathrm{V}} = \left(\frac{B}{C}\right)^{1/2v} = \left(\frac{\varepsilon_s}{\varepsilon_\infty}\right)^{1/2v} \frac{1}{2\pi\tau} \tag{19}$$

and always is shifted to the high-frequency region because of the ratio $\varepsilon_s/\varepsilon_\infty \gg 1$.

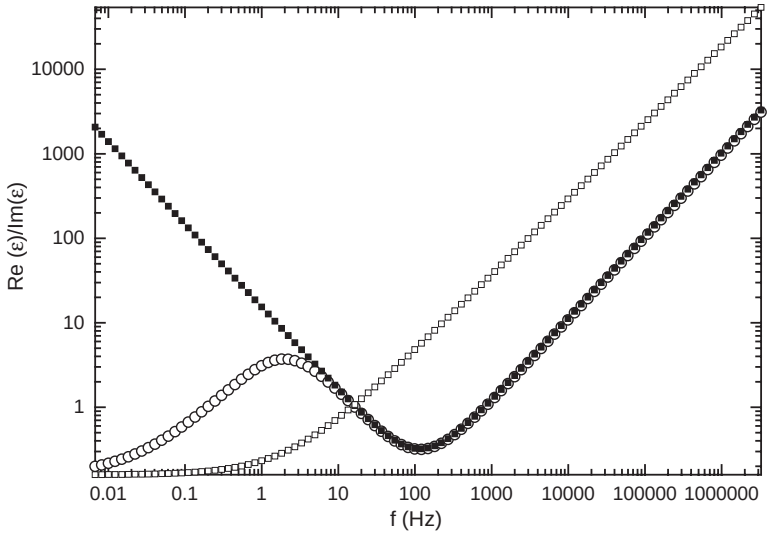

Fig. 3. Open circles represent the combination of LFD and Cole–Cole function, with parameters $\nu_{\text{Cole–Cole}} = 0.98$, $\tau_{\text{Cole–Cole}} = 0.01$, $\varepsilon_s = 350$, $\varepsilon_\infty = 7$, $\tau_{\text{LFD}} = 0.001$, $\alpha = 0.9$. Open squares represent a single LFD with parameters $\tau_{\text{LFD}} = 0.001$, $\alpha = 0.9$, $\varepsilon_s = 7$. Solid squares represent a 'pure' Cole–Cole function with parameters $\nu_{\text{Cole–Cole}} = 0.98$, $\tau_{\text{Cole–Cole}} = 0.01$, $\varepsilon_s = 350$, $\varepsilon_\infty = 7$.

Ratio format for the combination of an LFD and Cole–Cole function: The general expression for the complex permittivity of a linear combination of the Cole–Cole function and the LFD is described by

$$\varepsilon(\mathrm{j}\omega) = \varepsilon_\infty + \frac{\sigma}{(\mathrm{j}\omega)^\alpha} + \frac{\Delta\varepsilon}{1 + (\mathrm{j}\omega\tau)^\nu}. \tag{20}$$

Presentation in the RP format leads to the expression

$$-\left(\frac{\mathrm{Re}[\varepsilon(\mathrm{j}\omega)]}{\mathrm{Im}[\varepsilon(\mathrm{j}\omega)]}\right) = \frac{A + Bf^{\nu_1} + Cf^{\nu_2} + Df^{\nu_1+\nu_2} + Ef^{2\nu_2} + Ff^{2\nu_2+\nu_1}}{G + Hf^{\nu_2} + If^{\nu_1+\nu_2} + Jf^{2\nu_2}}, \tag{21}$$

where $\omega = 2\pi f$, $\Delta\varepsilon = \varepsilon_s - \varepsilon_\infty$, and A, B, C, D, E, F, G, H, I and J are constants determined by initial parameters entering into the previous expression (20). The analytical relationships between the conventional parameters and these new parameters are rather cumbersome and are not given in this paper. However, the visual presentation of expression (21) allows one to notice a peak created by the combination of these two processes that provides evidence of the coexistence of two processes (see Fig. 3).

Ratio format for the combination of an LFD and two Cole–Cole functions: The general expression for the complex permittivity of a linear combination of the two Cole–Cole functions and the LFD is described by

$$\varepsilon(\mathrm{j}\omega) = \varepsilon_\infty + \frac{\sigma}{(\mathrm{j}\omega)^\alpha} + \frac{\Delta\varepsilon_1}{1 + (\mathrm{j}\omega\tau_1)^{\nu_1}} + \frac{\Delta\varepsilon_2}{1 + (\mathrm{j}\omega\tau_2)^{\nu_2}}, \tag{22}$$

where $\omega = 2\pi f$, $\Delta\varepsilon = \varepsilon_s - \varepsilon_\infty$. Application of the RP format leads to a quite complex expression and is not given here. However, the visual presentation of expression (22) allows one to see again the invariable form of the double V-shaped function depicted in Fig. 4 (arrows 1 and 2) created by the additive combination of the two Cole–Cole processes and a peak (arrow 3) created by the contribution of LFD process.

Ratio format for the series combination of two recap elements: The general expression for the complex permittivity combined by of two recap elements, in series, is given by Eq. (5) with $R(\mathrm{j}\omega)$ from (6b). The application of the RP format to this function leads to

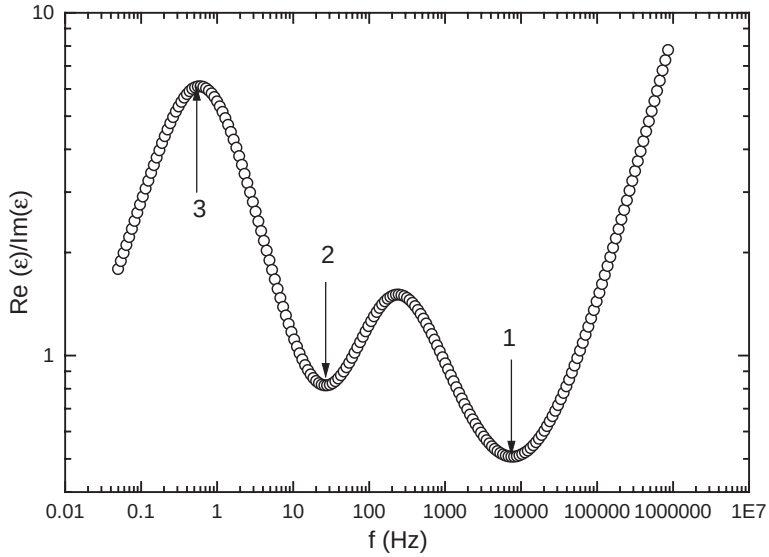

Fig. 4. Open circles represent the linear combination of LFD and two Cole–Cole functions in RP format, with parameters $\nu_{\text{Cole–Cole1}} = 0.85$, $\tau_{\text{Cole–Cole1}} = 0.0002$, $\varepsilon_{s1} = 100$, $\nu_{\text{Cole–Cole2}} = 0.95$, $\tau_{\text{Cole–Cole2}} = 0.02$, $\varepsilon_{s2} = 800$, $\varepsilon_{\infty} = 2$, $\tau_{\text{LFD}} = 0.001$, $\alpha = 0.8$. Arrows 1 and 2 show the first and second Cole–Cole processes as inverted peaks, and arrow 3 shows the peak obtained as a the result of the combination of the second Cole–Cole peak with LFD function.

the expression

$$\frac{\text{Re}[\varepsilon(\text{j}\omega)]}{\text{Im}[\varepsilon(\text{j}\omega)]} = \frac{A+Bf^{\nu_1}+Cf^{\nu_2}+Df^{\nu_1+\nu_2}+Ef^{\nu_1-\nu_2}+Ff^{-\nu_1+\nu_2}}{Gf^{\nu_1}+Hf^{\nu_2}}. \tag{23}$$

Numerical verification of expression (23) shows that the function describes a single asymmetric peak. Fig. 5 clearly demonstrates this asymmetric behavior (which is characterized by the downward displacement of the high-frequency branch), obtained for a model spectrum. Here the asymmetry always appears on the *right* side of V-shaped function. This asymmetry therefore differentiates between a model defined by two recap elements combined in series and a model defined by a single Cole–Cole function, which is characterized by mirror-like symmetry with respect to the minimum frequency.

Ratio format for the parallel combination of two recap elements: The general expression for the complex permittivity for two recap elements, combined in parallel, is given by Eq. (5) with $R(\text{j}\omega)$ from (6a). Again, the application of the RP format leads to the expression

$$-\left(\frac{\text{Re}[\varepsilon(\text{j}\omega)]}{\text{Im}[\varepsilon(\text{j}\omega)]}\right) = \frac{A+Bf^{\nu_1}+Cf^{\nu_2}}{Df^{\nu_1}+Ef^{\nu_2}}, \tag{24}$$

where $\omega = 2\pi f$, A, B, C, D and E are some constants determined by initial parameters of expression (5) with $R(\text{j}\omega)$ from (6a). Numerical verification of expression (24) shows that the function describes also a single asymmetric peak. Fig. 6 clearly demonstrates this asymmetric behavior (which is characterized by the downward displacement of the low-frequency branch), obtained for a model spectrum. Here the asymmetry always appears on the *left* side of the V-shaped function. This asymmetry therefore differentiates between a model defined by two recap elements combined in parallel from a model defined by a Cole–Cole function, which is characterized by mirror-like symmetry with respect to the minimum frequency and a model defined by two recap elements in series, which is characterized by right-hand asymmetry.

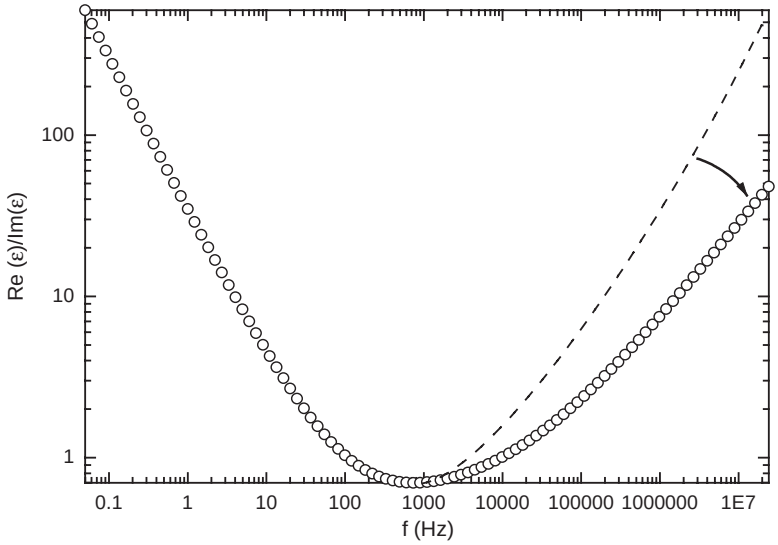

Fig. 5. The RP format for two recap elements combined in series. They are described by function (5) with $R(j\omega)$ from (6b) with parameters: $v_1 = 0.98$, $\tau_1 = 0.005$, $v_2 = 0.6$, $\tau_2 = 0.01$, $\varepsilon_s = 200$, $\varepsilon_\infty = 1.5$. Dashed line shows the position of the high-frequency branch in the case of the negligible influence of the second process (provided by the second recap element). Arrow shows the movement of the high-frequency branch due to influence of the second process. Hence, we have a 'dropping' asymmetry due to the falling down of the high-frequency branch.

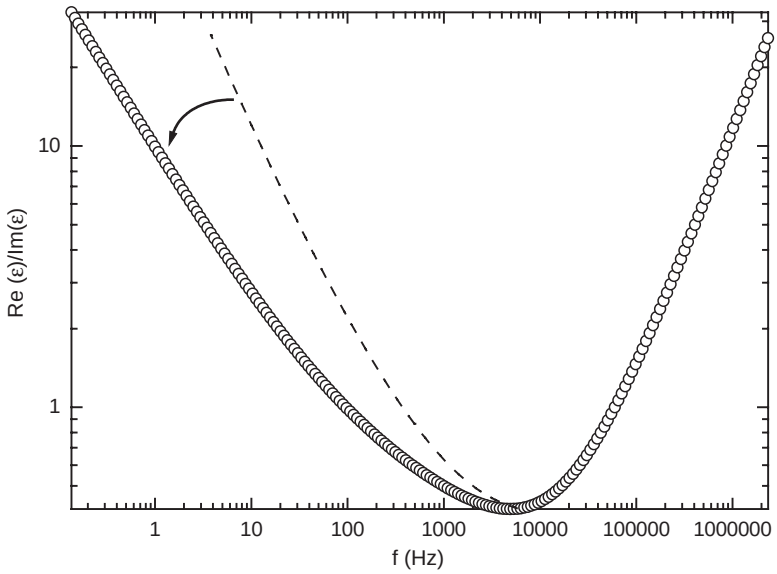

Fig. 6. The RP format for two recap elements combined in parallel. They are described by function (5) with $R(j\omega)$ from (6a) with parameters: $v_1 = 0.98$, $\tau_1 = 0.001$, $v_2 = 0.6$, $\tau_2 = 0.05$, $\varepsilon_s = 1000$, $\varepsilon_\infty = 2$. Dashed line shows the position of the low-frequency branch, when the influence of the second process (provided by the second recap element) is negligibly small. Arrow shows the movement of the low-frequency branch due to influence of the second process. Hence, we have a 'dropping' asymmetry due to falling down at the low-frequency branch.

General features of the ratio presentation format: This investigation shows that the RP format helps to differentiate, at least *qualitatively*, between different functions (including LFD, Cole–Cole and more complex functions presented by expression (5) (with the complex function $R(j\omega)$ from (6a) and (6b)), and their linear combinations.

For all functions considered above in the ratio format, one obtains all fitting parameters *simultaneously* for both parts of complex permittivity, except ε_∞ and ε_s. It follows from Table 1 that one can obtain reliable values only for the ratio $\varepsilon_s/\varepsilon_\infty$. This statement follows from definition (16). However, separate values of ε_∞ and ε_s can be obtained easily by fixing initially their ratio and then making one of the parameters float free (usually ε_s) until the best fit is obtained in the normal presentation format.

Finishing this section we would like to stress one important point. Expression (16) coincides with cotangent of dielectric loss and from the first sight it is not necessary to introduce new definition and define it as new format. As far as we know the 'old' format taken in the form of a tangent loss angle was *not* investigated properly in the sense of giving new additional information in comparison with usual presentation of DS data. The logarithm taken from cotangent loss angle gives new possibilities in differentiation of a true LFD process from a 'tail' of relaxation process with a peak located out admissible frequency window. That is why it has a sense to determine this presentation as a new RP format.

4. Separation procedure

Identification of the actual combination of the physically meaningful *recap* elements can be achieved relatively easily by employing the ECs data curve-fitting method [1,14,15] in conjunction with a proper analytical procedure to separate the contributions of the different *recap* elements to the dielectric permittivity/impedance functions describing the observed behavior. This procedure helps in differentiation of the complex permittivity functions expressed by formulae (5) with (6a) or (6b) in the form of linear combination of power-law functions. Both functions give an asymmetric peak, but their asymmetry is different. The first function (5) with (6a) creates an asymmetric broadening near the low-frequency branch, while the second combination (5) with (6b) creates an asymmetric broadening at the high-frequency branch. But for the case of a small asymmetry, when the contribution of the second process entering either in combination of (5) with (6a) or (5) with (6b) is *small*, it is quite difficult to decide what is the type of asymmetry we have. This problem related to detection of small asymmetry contribution can be resolved by the use of the following treatment. Let us express the initial complex permittivity function in the following form:

$$\varepsilon(j\omega) = \varepsilon_s - \frac{\Delta\varepsilon}{1 + R^{-1}(j\omega)} = \varepsilon_\infty + \frac{\Delta\varepsilon}{1 + R(j\omega)}, \quad (25)$$

where complex relaxation function $R(j\omega)$ combining all possible processes can be expressed either

$$R(j\omega) = (j\omega\tau_1)^{\nu_1} + (j\omega\tau_2)^{\nu_2} \quad (26a)$$

or

$$R^{-1}(j\omega) = (j\omega\tau_1)^{-\nu_1} + (j\omega\tau_2)^{-\nu_2}. \quad (26b)$$

Relationship (25) can be transformed, respectively, into a couple of equations

$$1 + R(j\omega) = \frac{\Delta\varepsilon}{\varepsilon(j\omega) - \varepsilon_\infty}, \quad (27a)$$

$$1 + R^{-1}(j\omega) = \frac{\Delta\varepsilon}{\varepsilon_s - \varepsilon(j\omega)}. \quad (27b)$$

These equations can help to distinguish between spectra formed by combination (25) with (26a) from another possible combination (25) with (26b). The imaginary parts of the left sides of Eqs. (27) form a linear combination of two power-law functions for $R(j\omega)$ (as expressed by (26a) or by (26b), respectively), it follows that these two power-law functions can be easily recognized by the use of the *separation procedure* firstly used in papers [1].

The separation procedure implies the multiplication of the right sides of equations (27a) and (27b) by the factor ω^{α_d}, where α_d (defined as separation exponent) should be located between ν_1 and ν_2 with opposite sign. For both cases of spectra from Eq. (25) with (26a) and (25) with (26b), this procedure should give the U-shaped curve. However, if we pass the spectrum formed by Eq. (25) with (26a) through the right part of Eq. (27b) then instead of U-shaped curve we

obtain a 'hump' at any values of separation exponent. Similarly, if we pass the spectrum formed by combination (25) with (26b) through the right part of Eq. (27a) (which is 'tuned' for recognition of functions (25), (26b)) then it becomes impossible to obtain the desired U-shaped curve (again no matter what a value is chosen for α_d).

For realization of the separation procedure and proper usage of expressions (25) it is necessary to know initial values of ε_s and ε_∞. For finding of their initial values one can use the presentation of the real part of complex permittivity in normal and modulus $(1/\varepsilon(j\omega))$ formats, respectively. If an admissible dielectric spectrum is located in frequency window

$$\omega_{\min} \leqslant \omega \leqslant \omega_{\max}, \tag{28a}$$

then initial values of ε_s and ε_∞ can be found from expressions

$$\varepsilon_s = \max(\mathrm{Re}\,\varepsilon(j\omega_{\min}), [\mathrm{Re}(1/\varepsilon(j\omega_{\min})]^{-1}),$$
$$\varepsilon_\infty = \min(\mathrm{Re}\,\varepsilon(j\omega_{\max}), [\mathrm{Re}(1/\varepsilon(j\omega_{\max})]^{-1}). \tag{28b}$$

Usually the values obtained in these two formats do not coincide with each other, so after their separate calculations it is necessary to take their extreme values as it shown by last expression.

One can stress also a useful property of complex function $R(j\omega)$, which helps to find the necessary corrections to the values of ε_s and ε_∞ defined by expression (28b). It easy to notice that at the given range of frequencies this function should have *monotonic* behavior, i.e. $R(j\omega) \to \infty$ (at $\omega \to \infty$) and $R(j\omega) \to 0$ (at $\omega \to 0$). Model calculations show that the corrected values of ε_s and ε_∞, obtained from the condition that behavior of the complex function $R(j\omega)$ should be positive and monotonic, are very close to the given ones, in spite of the fact that 'true' values of ε_s and ε_∞ are located out from frequency window and cannot be calculated with the use of conventional non-linear fitting procedure.

This separation procedure can help to reveal a presence of a small process between two large recognized processes. If this intermediate hidden process takes place then after realization of the separation procedure we obtain the U-shaped curve with a small 'hump' located between two raising limiting branches. The number of local humps identified with the help of separation procedure at certain value of α_d can help in identification of a *true* structure of kinetic equation (15) for the concrete dielectric material under consideration.

5. Analysis of available experimental data

In this section, we shall try to apply the previously developed additional procedures for treatment of available raw experimental data measured for complex permittivity.

The raw DS data were obtained for salol and have been measured in laboratory of F. Kremer (Faculty of Physics and Geology, Leipzig University, Leipzig, Germany). Figs. 7 and 8 show by open figures the real and imaginary parts of complex permittivity for salol at several temperatures. Fig. 9 shows the same spectra in ratio presentation (RP) format. Analyzing this picture one can notice at least two processes, *viz.*, high-frequency process (arrows 1) and low-frequency process (arrows 2). As for low-frequency process the normal presentation (Figs. 7 and 8) does *not* allow to determine whether it is a 'true' LFD or a 'tail' of some process with the peak (in normal presentation) located at the lower frequency range outside of the experimental frequency window. This question can be resolved with the help of the RP format. RP format depicted in Fig. 9 shows that the low frequency process is the linear combination of the LFD-type process and Cole–Cole-type process with the peak (in normal presentation) located at the lower frequency outside of the experimental frequency window. Arrow 3 points at the V-shaped curve at the lowest frequency region. So in accordance with the properties of RP format it can be identified as the Cole–Cole process.

Next step is the use of the separation procedure. Fig. 10 shows the result of the application of the separation procedure (case (27b)) to the initially identified high-frequency process. On this picture one can see the identified U-shaped curve with a small hump between two branches. But this hump is so small that we can neglect it in future analysis. Application of the separation procedure for Eq. (27a) cannot give the U-shaped curve. This analysis gives us evidence that in this case (for high-frequency process) there are at least two processes with complex permittivity

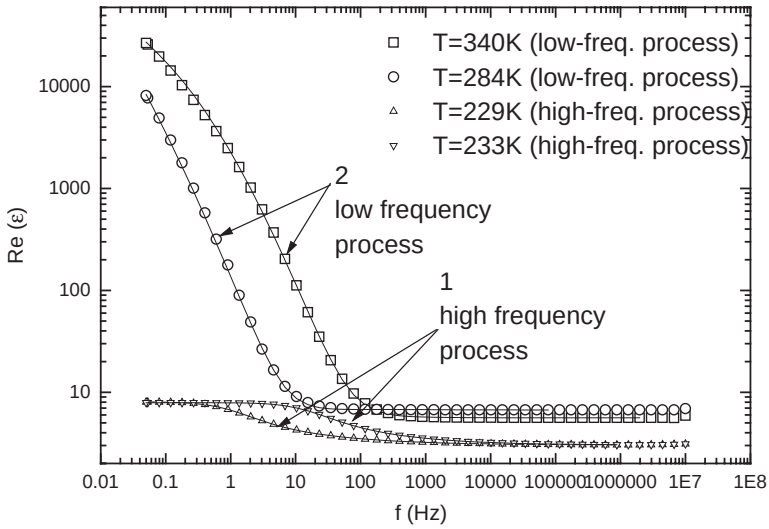

Fig. 7. Open figures and solid lines represent the *real* parts of complex permittivity for salol (phenyl salicylate $C_{13}H_{10}O_3$) (by F. Kremer) and correspondingly fitting curves obtained by the fitting procedure with the use of Eqs. (29), (30) (separately for low- and high-frequency regions) at some temperatures. Arrows 1 and 2 show the high- and low-frequency processes.

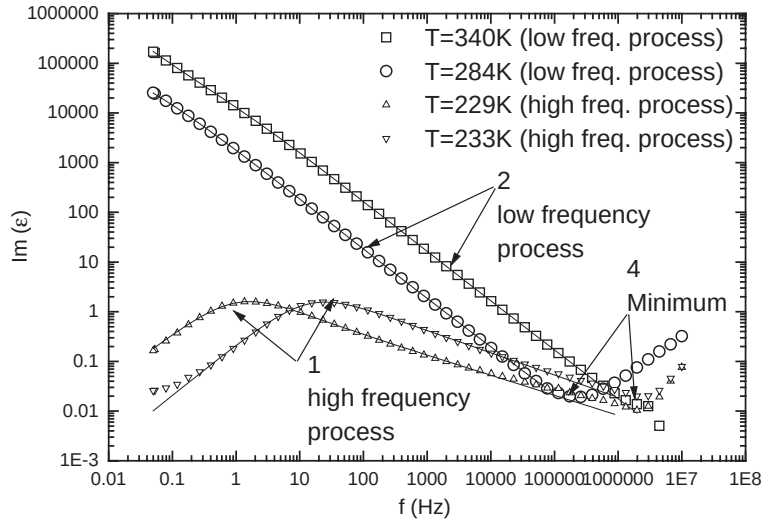

Fig. 8. Open figures and solid lines represent the *imaginary* parts of complex permittivity for the salol and correspondingly fitting curves obtained by the fitting procedure with the use of Eqs. (28), (29) (Separately for low- and high-frequency regions) for several temperatures. Arrows 1 and 2 show the high- and low-frequency processes. Two arrows (4) show the minimum between two processes.

expressed by the formula:

$$\varepsilon_1(j\omega) = \varepsilon_{1_\infty} + \frac{\Delta\varepsilon_1}{1 + R_1(j\omega)}, \tag{29a}$$

$$R_1^{-1}(j\omega) = (j\omega\tau_1)^{-\nu_1} + (j\omega\tau_2)^{-\nu_2}. \tag{29b}$$

As it has been detected previously in the RP format the low-frequency process of the Cole–Cole type (see Fig. 9) has the V-shaped identified curve with admixture of asymmetric part. This gives us an evidence to say that the low-frequency part of spectra can be

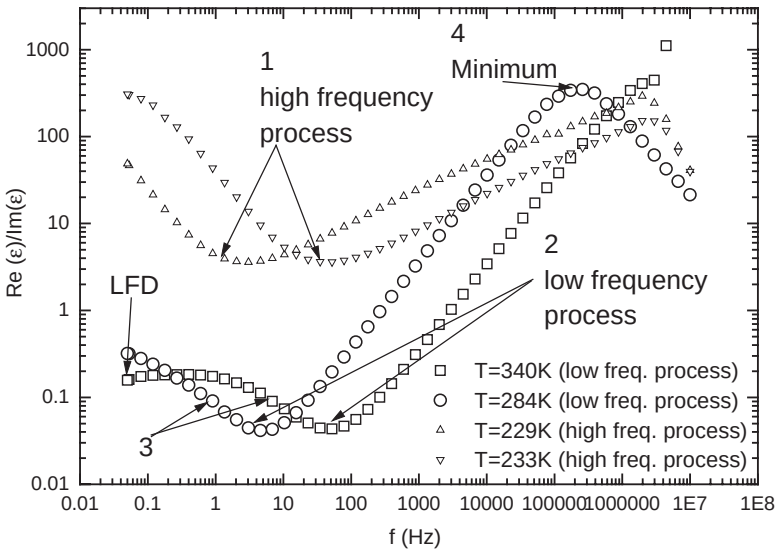

Fig. 9. The RP format for complex permittivity of the salol for several temperatures. Arrows 1 and 2 show the high- and low-frequency processes. Arrow 3 shows the V-shaped asymmetric curve.

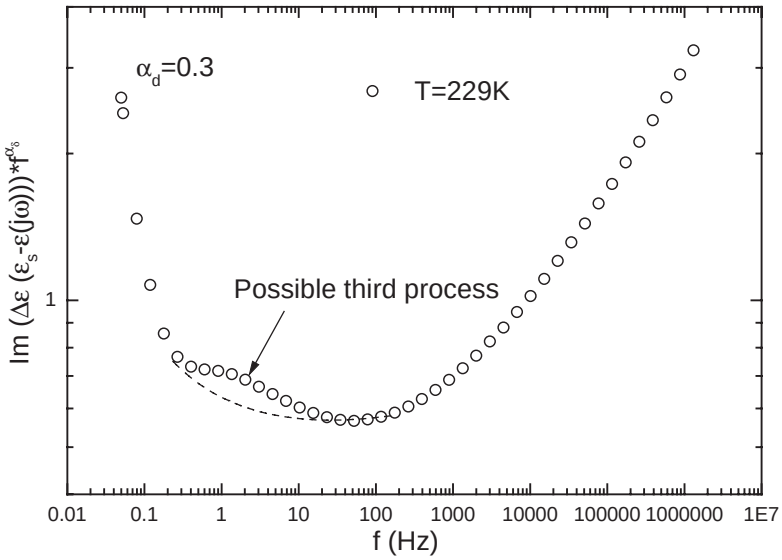

Fig. 10. Open squares with solid line represent the imaginary part $\mathrm{Im}(\Delta\varepsilon/\varepsilon_s-\varepsilon(j\omega))f^{\alpha_d}$ for the salol at the temperature $T=229.15$ K. $\alpha_d=0.3$. The dashed line shows the behavior for the case when the third process is absent. The shown arrow points out the third process.

described by the linear combination of the LFD and complex function with two recaps combined in parallel. So the complex permittivity function is expressed by the formula:

$$\varepsilon_2(j\omega)=\varepsilon_{2_\infty}+\frac{\sigma}{(j\omega)^{\alpha}}+\frac{\Delta\varepsilon_2}{1+R_2(j\omega)}, \tag{30a}$$

$$R_2(j\omega)=(j\omega\tau_3)^{\nu_3}+(j\omega\tau_4)^{\nu_4}. \tag{30b}$$

All possible measured frequency data for salol were fitted by the use of Eqs. (29) and (30). (Separately for low- and high-frequency regions). The results of the fitting procedure for some temperatures are shown in Figs. 7 and 8 by solid lines. The temperature

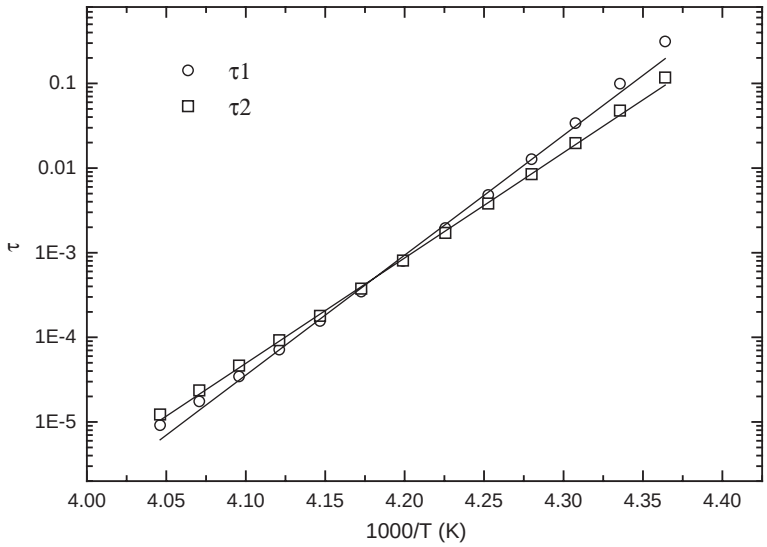

Fig. 11. Open figures and solid lines represent the temperature dependencies of the first and second relaxation times (high-frequency process) for the salol and correspondingly fitting curves obtained by the fitting procedure with the use of the conventional Arrhenius equation. The chosen fitting function and the results of the fitting procedure (values of the fitting parameters) for these data are collected in Table 2.

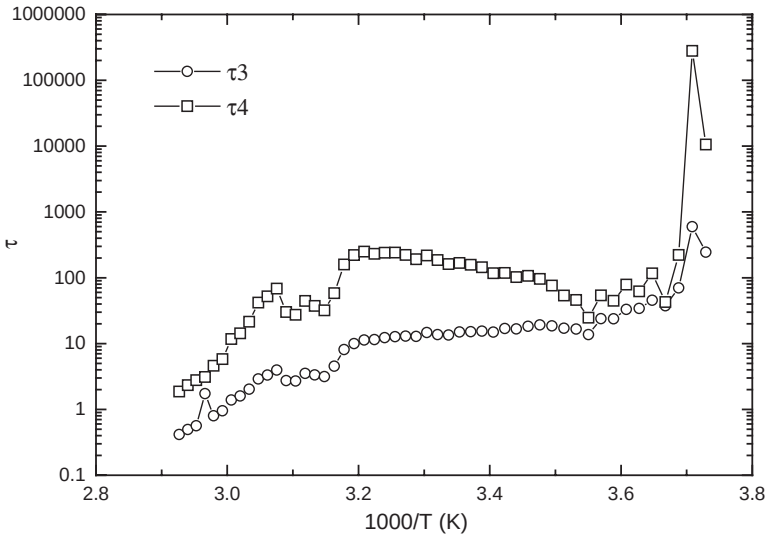

Fig. 12. Open figures and solid lines represent the temperature dependencies of the third and fourth relaxation times (low-frequency process) for the salol.

dependencies of the characteristic relaxation times are shown in Fig. 11 (for high-frequency process) and Fig. 12 (for low-frequency process). The temperature dependence of the first and the second relaxation times has simple Arrhenius behavior. The results of the fitting procedure with the use of Arrhenius equation are also shown in Fig. 11 by solid lines. The parameters obtained from these fitting procedures are collected in Table 2. As for the third and fourth relaxation times they have very unusual (close to random)

Table 2
The fitting parameters describing temperature dependence of relaxation times

Data	Fitting function	Fitting parameters
Salol τ_1	Ordinary Arrhenius	$\tau_A = 2.8 \times 10^{-63}$ $E = 32632$
Salol τ_2	Ordinary Arrhenius	$\tau_A = 4.1 \times 10^{-56}$ $E = 28686$
Pure glycerol τ_1	Generalized Arrhenius (32)	$\tau_A = 7.9 \times 10^{-49}$ $\tau(\infty) = \tau_A \exp(C) \sim \infty$ $E = 23751$ $C = 6.26 \times 10^{18}$ Hd = 9211
Pure glycerol τ_2	Generalized Arrhenius (32)	$\tau_A = 4 \times 10^{-55}$ $\tau(\infty) = \tau_A \exp(C) \sim \infty$ $E = 23568$ $C = 1200$ Hd = 1055
Pure glycerol τ_3	Generalized Arrhenius (32)	$\tau_A = 1.65 \times 10^{-163}$ $\tau(\infty) = \tau_A \exp(C) = 2.3 \times 10^{17}$ $E = 47746$ $C = 414.8$ Hd = 223.8

temperature behavior, which cannot be described by simple Arrhenius relationship. This dependence gives us an evidence to state that low- and high-frequency parts of this dielectric spectrum might have completely different physical nature.

The second set of experimental data for pure glycerol was obtained in laboratory of Prof. Y. Feldman (Hebrew University, Israel). Figs. 13 and 14 show by open figures the real and imaginary parts of complex permittivity of pure glycerol for several temperatures. Fig. 15 shows the same spectra in RP format. Analyzing these pictures one can notice at least two processes: high-frequency process (arrows 1) and low-frequency process (arrows 2). As for low-frequency process the normal presentation (Figs. 13 and 14) does *not* allow to determine whether it is an LFD or a 'tail' of some process with the peak (in normal presentation) located at the lower frequency outside of the experimental frequency window. This question can be resolved with the help of the RP format. RP format depicted in Fig. 15 shows that the low-frequency process is the Cole–Cole-type process with the peak (in normal presentation) located at the lower frequency *outside* of the experimental frequency window. Arrow 3 points out to a small U-turn at the lowest frequency region. So, in accordance with the properties of RP format it can be identified as a Cole–Cole process.

Next step is the usage of the separation procedure. Fig. 16 shows the result of the application of the separation procedure (case (27b)). On this picture one can see the U-shaped curve with small hump between two branches. Application of the separation procedure for Eq. (27a) cannot give the V-shaped curve. This gives us evidence to say that in this case we can have at least three processes with complex permittivity expressed by formulae:

$$\varepsilon(\mathrm{j}\omega) = \varepsilon_\infty + \frac{\Delta\varepsilon}{1 + R(\mathrm{j}\omega)}, \tag{31a}$$

$$R^{-1}(\mathrm{j}\omega) = (\mathrm{j}\omega\tau_1)^{-\nu_1} + (\mathrm{j}\omega\tau_2)^{-\nu_2} + (\mathrm{j}\omega\tau_3)^{-\nu_3}. \tag{31b}$$

All possible frequency data for pure glycerol were fitted by the use of Eq. (31) without low-frequency identified process expressed probably by Cole–Cole function. (the existing non-linear fitting software

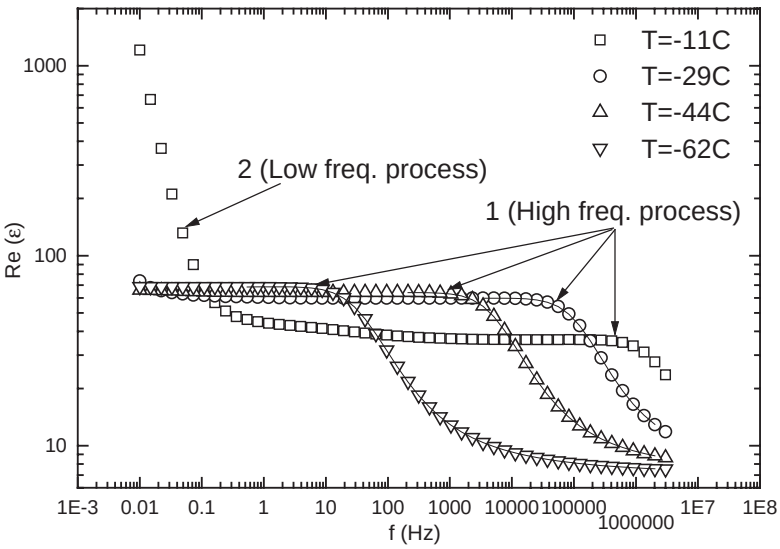

Fig. 13. Open figures and solid lines represent the *real* parts of complex permittivity for pure glycerol and correspondingly fitting curves obtained by the fitting procedure with the use of the equivalent scheme with three recap elements in series (Eqs. (31)) for several temperatures. Arrows 1 and 2 show the high- and low-frequency processes.

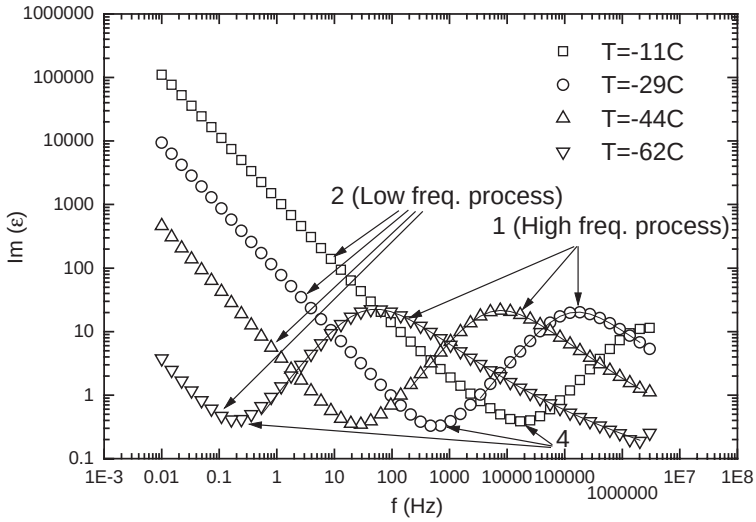

Fig. 14. Open figures and solid lines represent the *imaginary* parts of complex permittivity for pure glycerol and correspondingly the fitting curves obtained by the fitting procedure with the use of the equivalent scheme with three recap elements in series (Eqs. (31)) for several temperatures. Arrows 1 and 2 show the high- and low-frequency processes. Arrows 4 show the minimum between two processes.

does not allow fitting finally the whole curve including low-frequency part). The fitting procedure realized with the help of Eq. (31) describes quite well these raw experimental data. That is why for fitting procedures with these data we chose the equivalent scheme incorporating three recap elements. The results of the procedure for some temperatures are shown in Figs. 13 and 14 by solid lines. The

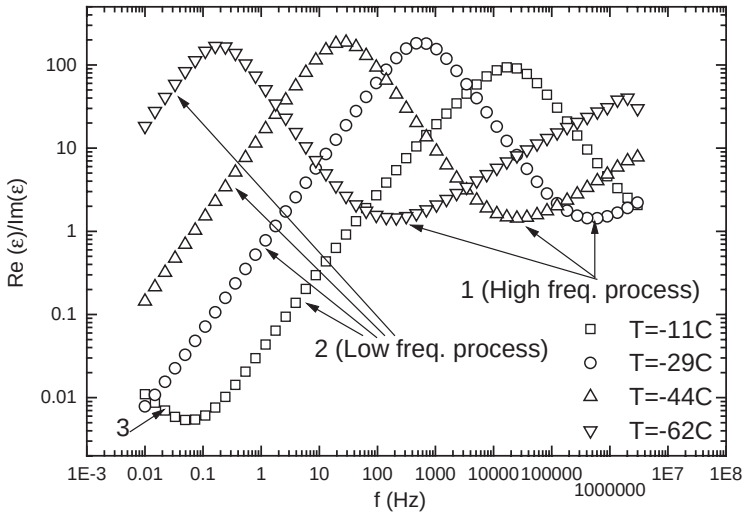

Fig. 15. The RP format for complex permittivity of pure glycerol for several temperatures. Arrows 1 and 2 show the high- and low-frequency processes. Arrow 3 shows the upturn on low frequency, which reflects a 'tail' of low-frequency process of the Cole–Cole type.

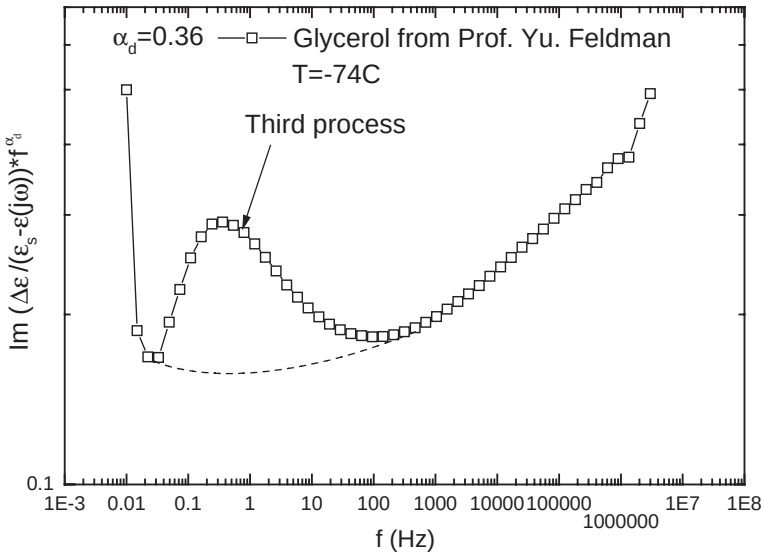

Fig. 16. Open squares with line represent the imaginary part of the $\Delta\varepsilon/(\varepsilon_s - \varepsilon(j\omega))f^{\alpha_d}$ for pure glycerol data at the temperature $T = -74°C$. $\alpha_d = 0.36$. Dashed line shows the behavior in case of absence of the third process. The arrow points out on the third process.

temperature dependencies of the characteristic relaxation times are shown in Fig. 17. All three relaxation times for pure glycerol have non-Arrhenius temperature dependencies. Moreover, the first process with the longest relaxation time demonstrates a possible critical point at the temperature $T \sim 232$ K.

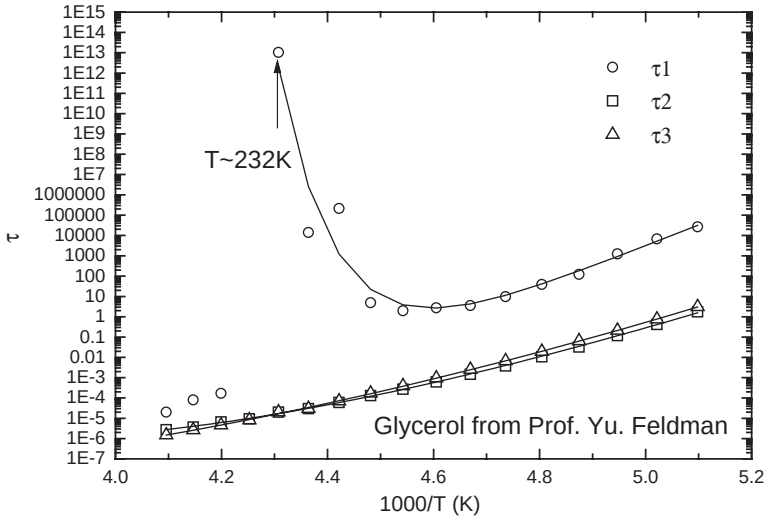

Fig. 17. Open figures and solid lines represent the temperature dependencies of the three relaxation times for pure glycerol and correspondingly fitting curves obtained by the fitting procedure with the use of the generalized Arrhenius equation (32). Arrow points out on the possible critical temperature. The chosen fitting function and the results of the fitting procedure (values of the fitting parameters) for these data are collected in Table 2.

Such temperature behavior of the relaxation time can be described by the generalized Arrhenius formula, suggested in [20]:

$$\tau(T) = \tau_{\mathrm{A}} \exp\left(\frac{E}{T} + C \exp\left[-\frac{H_{\mathrm{d}}}{T}\right]\right). \tag{32}$$

The results of the fitting procedure with the use of this equation are also shown in Fig. 17 by solid lines. The parameters obtained from these fitting procedures are collected in Table 2.

6. Results and discussion

The signal processing in dielectric spectroscopy is started from identification of a 'true' fitting function for description of the measured complex permittivity/impedance data. The conventional procedure of choosing of an appropriate empirical function for the fitting of raw DS data in available frequency/temperature range is not well justified in dielectric spectroscopy. Usually for the fitting of frequency data experimentalists frequently use the analytical functions (2) or (3) or their linear combinations. But description of frequency data by linear combinations of dielectric functions in general is *not* correct and can be considered only as *approximate* procedure. It can be justified only in the case when we have two different physical phenomena as, for example, an independent contribution of conductivity (LFD process) or possible electrode polarization process affecting the total relaxation process in a bulk material. Usually the additive hypothesis can be justified in resonance spectroscopy for well-resolved resonance lines, but in dielectric spectroscopy where two peaks can form frequently one asymmetrical peak this 'blind' copying is far from real data fitting. The case is that any complex dielectric spectra is closely related to the corresponding kinetic equation for the *total* macroscopic polarization and to obtain the unique kinetic equation from additive combination of simple complex susceptibilities given, for example, by expressions (2) or (3) represents an unsolved problem. The general expression for complex permittivity of type (5), where the unified complex relaxation function $R(\mathrm{j}\omega)$ can have an arbitrary structure really corresponds to the structure of a possible kinetic equation for the total value of macroscopic polarization in time domain. From this point of view for each expression (1), (2) and (3) the corresponding kinetic equation can be easily found. But

unfortunately, experimental verifications show that these expressions taken in a single form cannot describe the whole dielectric spectra in a set of heterogeneous materials. It would be desirable to find a 'pattern' material, which exactly corresponds to a single HN function but the eigen-coordinates found in [15b] and specially 'tuned' for recognition of this function did not show its presence in available data analyzed. The identified functions (6) describing raw DS data give us a chance to construct true kinetic equations for describing of dielectric relaxation in wide class of heterogeneous materials.

Analysis made on real salol and pure glycerol data confirms the existence of new kinetic equations of type (15). The identified function (31) for pure glycerol representing the stationary solution allows in restoring the corresponding kinetic equation in time domain. It can be written in two equivalent forms

$$[\tau_1^{-\nu_1} D_{t_0}^{-\nu_1} + \tau_2^{-\nu_2} D_{t_0}^{-\nu_2} + \tau_3^{-\nu_3} D_{t_0}^{-\nu_3}] \times (P(t) - P(t_0)) + P(t) = 0 \quad (33a)$$

or

$$[\tau_1^{-\nu_1} D_{t_0}^{-\nu_1} + \tau_2^{-\nu_2} D_{t_0}^{-\nu_2} + \tau_3^{-\nu_3} D_{t_0}^{-\nu_3}]^{-1} P(t) + [P(t) - P(t_0)] = 0. \quad (33b)$$

It is interesting to note that the second form of this kinetic equation contains a differential operator, which represents itself the inverse operator to a linear combination of fractional *integral* operators. This unexpected result and the corresponding type of kinetic equation have a general interest and can be important for understanding of kinetic phenomena at whole. Without recognized of a low-frequency process this kinetic equation describes the relaxation process in pure glycerol. It is interesting to note that this identified kinetic equation naturally defines the relaxation times of possible subsystems involved in the relaxation process and allows in finding their possible temperature dependencies based on very simple model suggested in paper [20]. The separation procedure allows in identifying of three relaxation processes taking place in pure glycerol. This is quite new result that needs in more careful analysis and further confirmations based on structural peculiarities of this substance.

We want to stress here that attempts to write true kinetic equations were realized by many researches. One can remind the cluster theory of Dissado and Hill [8], which unfortunately did not receive the further development because the obtained expression for complex susceptibility function did not describe well the DS data and the physical meaning of theoretical parameters figuring in the D–H cluster theory was not clear. The mode-coupling theory [2] pretending to description of DS data in glass-forming materials cannot give complete description of DS data [11] and now it is in the stage of experimental verification. Eq. (15) can be considered at the initial stage as phenomenological kinetic equation, which reflects the fractal structure of subsystems involved in the process of relaxation. Now it is difficult to derive this equation microscopically but nevertheless it is possible to understand the physical meaning of fractional integral which appears in the result of averaging of a smooth function (in the given case the total polarization) over the fractal set [13].

In conclusion we would like to point out that with the use of the RP format and separation procedure on can recognize a structure of the desired kinetic equation and the corresponding fitting function in frequency domain (equivalent scheme). After recognition the fitting procedure was realized by the use of conventional non-linear least-squares method. And this fact put forward a problem of determination of the 'global' minimum and searching the 'true' values (physically meaningful) for parameters through the fitting procedure. As it is well-known [5] non-linear fitting procedure depends in greater extend on the initial values of the fitting parameters and this dependence increases with increasing of the number of fitting parameters. In our case, we have quite large number of parameters that complicate the fitting procedure. To determine the range for initial values for some fitting parameters (τ and ν) we used the so-called EC's method [1,14,15] together with separation procedure i.e. we made the fitting procedures based on EC's method on U-shaped curves, similar to that shown in Figs. 10 and 16. One of the basic features of the EC's method is the determination of a 'global' minimum in the realized fitting procedure. It becomes important when we do *not* know a priori initial values of parameters, especially in cases, when the number of the fitting parameters is sufficiently large. Another important feature of the EC's method is a possibility in detection of the most suitable analytical hypothesis among other proposed hypotheses

chosen for the fitting of real experimental data. In the EC's representation, the EC's plots corresponding to a 'true' function should give a set of sloping lines with fitting constants that enter into a basic relationship by a *linear* way. They are related algebraically to the initial set of the fitting parameters of the original function considered. So it becomes possible to use reliable (close to the desired global minimum) initial values for τ and ν and perform the non-linear fitting procedure for the whole complex function.

Acknowledgements

One of us (R.R.N) wants to express his acknowledgements to Prof. F. Kremer (Faculty of Physics and Geology, Leipzig University, Leipzig, Germany) and Prof. Yu. Feldman (Hebrew University, Israel) for available DS data sent for analysis.

References

[1] (a) M.M. Abdul-Gader Jafar, R.R. Nigmatullin, Thin Solid Films 396 (2001) 280;
(b) R.R. Nigmatullin, M.M. Abdul-Gader Jafar, N. Shinyashiki, Seiichi Sudo, Shin Yagihara, J. Non-Crystalline Solids 305 (2002) 96.

[2] (a) U. Bengtzelius, W. Gotze, A. Sjolander, J. Phys. C 17 (1984) 5915;
(b) W. Gotze, L. Sjogren, Rep. Progr. Phys. 55 (1992) 241.

[3] R. Böhmer, K.L. Ngai, C.A. Angell, D.J. Plazek, J. Chem. Phys. 99 (1993) 4201.

[4] (a) Yu. Feldman, A. Andrianov, E. Polygalov, G. Romanychev, I. Ermolina, Yu. Zuev, B. Milgotin, Rev. Sci. Instrum. 67 (1996) 3208;
(b) Yu. Feldman, R. Nigmatullin, E. Polygalov, J. Texter, Phys. Rev. E 58 (1998) 7561.

[5] L. Graige, Global Non-Linear Optimization Method using Mathematica (version 4.0), Loehle Enterprises, Illinois, 1999.

[6] S. Havriliak Jr., S.J. Havriliak, Dielectric and Mechanical Relaxation in Materials, Carl Hanser, New York, 1997.

[7] A. Hofmann, F. Kremer, E.W. Fischer, A. Schönhals, in: R. Richert, A. Blumen (Eds.), Disordered Effects on Relaxation Processes, Springer, Berlin, 1994, p. 309.

[8] (a) A.K. Jonscher, Dielectric Relaxation in Solids, Chelsea Dielectric Press, London, 1983;
A.K. Jonscher, Universal Relaxation Law, Chelsea Dielectric Press, London, 1996;
A.K. Jonscher, J. Phys. D: Appl. Phys. 32 (1999) R57;
(b) A.K. Jonscher, J. Mater. Sci. 26, (1991) 1618;
(c) A.K. Jonscher, Colloid. Polym. Sci. 253 (1975) 231;
(d) A.K. Jonscher, Nature 253, (1975) 717;
A.K. Jonscher, Nature 256 (1975) 566;
A.K. Jonscher, Nature 267 (1977) 673;
R.M. Hill, Nature 275 (1978) 96;
K.L. Ngai, A.K. Jonscher, C.T. White, Nature 277 (1979) 185.

[9] R.L. Leheny, S.R. Nagel, Europhys. Lett. 39 (1997) 447.

[10] (a) P. Lunkenheimer, A. Pimenov, B. Schiener, R. Böhmer, A. Loidl, Europhys. Lett. 33 (1996) 611;
(b) P. Lunkenheimer, A. Pimenov, M. Dressel, B. Gorshunov, U. Schneider, B. Schiener, R. Böhmer, A. Loidl, Structure and dynamics of glasses and glass formers, in: C.A. Angell, K.L. Ngai, J. Kieffer, T. Egami, G.U. Nienhaus (Eds.), Materials Research Society Symposium Proceedings, Vol. 455, Pittsburgh, 1997, p. 47.

[11] P. Lunkenheimer, Dielectric Spectroscopy of Glassy Systems, Shaker Verlag, Augsburg, 1999.

[12] A. Le Mehaute, Fractal Geometries, Theory and Applications (translated by J. Howlett), Penton Press, London, 1991;
J. Feder, Fractals, Plenum Press, London, 1989;
L. Barabasi, H.E. Stanley, Fractal Concepts in Surface Growth, Cambridge University Press, Cambridge, 1995.

[13] A. Le Mehaute, R.R. Nigmatullin, L. Nivanen, Fleches du Temps et Geometrie Fractale, Hermes, Paris, 1998 (in French).

[14] R.R. Nigmatullin, Appl. Magnet. Resonance 14 (1998) 601.

[15] R.R. Nigmatullin, Physica A 285 (2000) 547.

[16] (a) G.A. Niklasson, J. Appl. Phys. 62 (1987) R1;
J.R. Macdonald, J. Appl. Phys. 62 (1987) R51;
G.A. Niklasson, J. Appl. Phys. 58 (1985) 1971;
(b) M. Strómme, J. Isidorsson, G.A. Niklasson, C.G. Granqvist, J. Appl. Phys. 80 (1996) 233.

[17] K.B. Oldham, J. Spanier, The Fractional Calculus, Academic Press, NY, London, 1974.

[18] W.H. Press, S.A. Teukolsky, W.T. Vetterling, B.P. Flannery, Numerical Recipes in Fortran, 2nd ed., Cambridge University Press, Cambridge, 1992;
P.R. Bevington, D.K. Robinson, Data Reduction and Error Analysis for the Physical Sciences, 2nd ed., McGraw-Hill, New York, 1992.

[19] V. Raicu, Phys. Rev. E 60 (1999) 4677.

[20] Ya.E. Ryabov, A. Gutina, V. Arkhipov, Yu. Feldman, J. Phys. Chem. B. 105 (2001) 1845–1850.

[21] (a) T. Sato, H. Niwa, A. Chiba, R. Nozaki, J. Chem. Phys. 108 (1998) 4138;
(b) N. Shinyashiki, S. Sudo, W. Abe, S. Yagihara, J. Chem. Phys. 109 (1998) 9843;
(c) N. Shinyashiki, I. Arita, S. Yagihara, S. Mashimo, J. Chem. Phys. B102 (1998) 3249.

[22] H. Schiessel, A. Blumen, J. Phys. A 26 (1993) 5057;
H. Schiessel, et al., J. Phys. A 28 (1995) 6567;
H. Schiessel, et al., in: R. Hilfer (Ed.), Applications of Fractional Calculus in Physics, World Scientific, Singapore, 2000, p. 331.

[23] (a) U. Schneider, P. Lunkenbeimer, R. Brand, A. Loidl, J. Non-Cryst. Solids 235 (1998) 173;
(b) Michio Tokuyama, Irwin Oppenheim (Eds.), Slow Dynamics in Complex Systems: Eighth Tohwa University

International Symposium, CP469, The American Institute of Physics, 1999.
[24] A. Schönhals, F. Kremer, A. Hofmann, E.W. Fischer, E. Schlosser, Phys. Rev. Lett. 70 (1993) 3459.
[25] (a) J.C. Wang, J.B. Bates, Solid State Ionics 50 (1992) 75; (b) C.J.F. Böttcher, P. Bordewijk, Theory of Electric Polarization, Vols. I & II, Elsevier, New York, 1978.